Journal of Pharmaceutical Analysis 14 (2024) 100–114

Contents lists available at ScienceDirect

Journal of Pharmaceutical Analysis

journal homepage: www.elsevier.com/locate/jpa

Original article

Distinct molecular targets of ProEGCG from EGCG and superior inhibition of angiogenesis signaling pathways for treatment of endometriosis

Sze Wan Hung [a, 1], Massimiliano Gaetani [b, c, d, 1], Yiran Li [a], Zhouyurong Tan [a], Xu Zheng [a], Ruizhe Zhang [a, e], Yang Ding [a], Gene Chi Wai Man [a], Tao Zhang [a], Yi Song [a], Yao Wang [a], Jacqueline Pui Wah Chung [a], Tak Hang Chan [f], Roman A. Zubarev [b, d, g, **], Chi Chiu Wang [a, h, i, j, *]

[a] Department of Obstetrics & Gynaecology, The Chinese University of Hong Kong, Hong Kong, China
[b] Division of Physiological Chemistry I, Department of Medical Biochemistry and Biophysics, Karolinska Institutet, Stockholm, SE 17177, Sweden
[c] Chemical Proteomics Core Facility, Department of Medical Biochemistry and Biophysics, Karolinska Institutet, Stockholm, SE 17177, Sweden
[d] Unit of Chemical Proteomics, Science for Life Laboratory (SciLifeLab), Stockholm, SE 17177, Sweden
[e] Center for Reproductive Medicine, Henan Key Laboratory of Reproduction and Genetics, The First Affiliated Hospital of Zhengzhou University, Zhengzhou, 450003, China
[f] Department of Chemistry, McGill University, Montreal, H3A2K6, Canada
[g] Department of Pharmacological & Technological Chemistry, I.M. Sechenov First Moscow State Medical University, Moscow, 119146, Russia
[h] Reproduction and Development, Li Ka Shing Institute of Health Sciences, The Chinese University of Hong Kong, Hong Kong, China
[i] School of Biomedical Sciences, The Chinese University of Hong Kong, Hong Kong, China
[j] Chinese University of Hong Kong-Sichuan University Joint Laboratory in Reproductive Medicine, The Chinese University of Hong Kong, Hong Kong, China

ARTICLE INFO

Article history:
Received 16 November 2022
Received in revised form
28 August 2023
Accepted 5 September 2023
Available online 11 September 2023

Keywords:
Molecular targets
ProEGCG
EGCG
Angiogenesis
Treatment
Endometriosis

ABSTRACT

Endometriosis is a common chronic gynecological disease with endometrial cell implantation outside the uterus. Angiogenesis is a major pathophysiology in endometriosis. Our previous studies have demonstrated that the prodrug of *epigallocatechin* gallate (ProEGCG) exhibits superior anti-endometriotic and anti-angiogenic effects compared to *epigallocatechin* gallate (EGCG). However, their direct binding targets and underlying mechanisms for the differential effects remain unknown. In this study, we demonstrated that oral ProEGCG can be effective in preventing and treating endometriosis. Additionally, 1D and 2D Proteome Integral Solubility Alteration assay-based chemical proteomics identified metadherin (MTDH) and PX domain containing serine/threonine kinase-like (PXK) as novel binding targets of EGCG and ProEGCG, respectively. Computational simulation and BioLayer interferometry were used to confirm their binding affinity. Our results showed that MTDH-EGCG inhibited protein kinase B (Akt)-mediated angiogenesis, while PXK-ProEGCG inhibited epidermal growth factor (EGF)-mediated angiogenesis via the EGF/hypoxia-inducible factor (HIF-1a)/vascular endothelial growth factor (VEGF) pathway. *In vitro* and *in vivo* knockdown assays and microvascular network imaging further confirmed the involvement of these signaling pathways. Moreover, our study demonstrated that ProEGCG has superior therapeutic effects than EGCG by targeting distinct signal transduction pathways and may act as a novel anti-angiogenic therapy for endometriosis.

1. Introduction

Endometriosis is a common gynecological disease characterized by the ectopic implantation of functional endometrial cells and tissues outside of the uterus, primarily in the ovaries or peritoneal cavity. Endometriosis affects approximately 10% of women of reproductive age [1]. More than 80% of women with endometriosis suffer from pelvic pain, dyspareunia, and dysmenorrhea [2];

Peer review under responsibility of Xi'an Jiaotong University.
* Corresponding author. Department of Obstetrics & Gynaecology, The Chinese University of Hong Kong, Hong Kong, China.
** Corresponding author. Division of Physiological Chemistry I, Department of Medical Biochemistry and Biophysics, Karolinska Institutet, Stockholm, SE 17177, Sweden.
E-mail addresses: roman.zubarev@ki.se (R.A. Zubarev), ccwang@cuhk.edu.hk (C.C. Wang).
[1] Both authors contributed equally to this work.

https://doi.org/10.1016/j.jpha.2023.09.005

meanwhile, 20%–30% of these patients will also experience infertility [3,4]. In addition to being a major medical burden, it generates great distress in patients, negatively impacting their quality of life and working productivity. Currently, the most widely plausible theory is Sampson's theory of retrograde menstruation, stating that viable endometrial cells reflux through the fallopian tubes during menstruation for implantation, growth, and infiltration in the peritoneal cavity [5]. Similarly, these endometrial cells can also circulate to ectopic sites via vascular dissemination [6]. Hence, angiogenesis is identified as one of the major pathophysiological and signal transduction pathways for the promotion of nutrients and oxygen supply to provoke the progression of endometriotic lesions [7].

Current treatments for endometriosis include surgical and medical therapies. However, both methods have limitations. In surgical therapy, it can harm other organs and cause postoperative recurrence [8]. Oral contraceptives and gonadotropin-releasing hormone (GnRH) can inevitably lead to hypoestrogenism [9,10]. Additionally, the use of medical therapies increase the risk of infertility, bone loss associated with long-term usage, and recurrence after discontinuation [11]. Given these limitations, an antiangiogenic approach has been proposed as a potential therapeutic regimen to treat endometriosis [12]. Anti-angiogenic inhibitor includes SU6668, sunitinib, sorafenib and pazopanib, which are multityrosine kinase inhibitors under preclinical studies [7]. These inhibitors induced regression of endometrial grafts by blocking vascular endothelial growth factor receptor (VEGFR), fibroblast growth factor receptors 1, or platelet-derived growth factor receptor β [13]. However, tyrosine kinase inhibitors have been associated with a significant risk of treatment toxicities [13]. Hence, there remains the need to find an ideal therapeutic agent for targeting angiogenic pathways with minimal side effects for the prevention and treatment of endometriosis.

In recent years, *epigallocatechin* gallate (EGCG), a polyphenol catechin from green tea, has been shown to have multiple targets, potentially bringing synergistic actions and superior efficacy to resolve the complex pathophysiology of endometriosis [7]. Previously, we demonstrated the efficacies of green tea EGCG and prodrug of *epigallocatechin* gallate (ProEGCG) in endometriosis *in vivo* [14–16]. ProEGCG showed greater bioavailability and efficacy than EGCG in inhibiting lesion development in endometriosis. This compound was found to have more potent anti-angiogenesis activities with no observable adverse effects on reproductive tissues. However, the direct binding targets and mediated signaling pathways that led to the superior efficacy of ProEGCG in inhibiting endometriosis growth and vascularization remain to be elucidated. In preclinical research, target identification is an essential step for optimizing pharmacological properties to maximize drug specificity and efficacy. The aim of this study was to demonstrate the efficacy of ProEGCG as an oral formulation for the prevention and treatment of endometriosis. We employed a chemical proteomics approach, the proteome integral solubility alteration (PISA) assay, to deconvolute the potential targets of ProEGCG. Moreover, this study can help to elucidate the effects of EGCG and ProEGCG on the binding targets and their signaling pathways during the growth and angiogenic development of endometriosis using *in vitro* and *in vivo* models. Our study provides an in-depth mechanism to evaluate the differentiated targets and mechanisms for the superior therapeutic effects of ProEGCG over EGCG as a novel antiangiogenic agent in inhibiting endometriosis.

2. Materials and methods

2.1. Chemicals

EGCG (purity ≥95%) was purchased from Sigma-Aldrich (St. Louis, MO, USA). ProEGCG (purity ≥99.8%, determined by liquid chromatography with tandem mass spectrometry (LC-MS/MS)) was a kind gift from The Polytechnic University of Hong Kong (Hong Kong, China) and prepared according to a previous report [17]. PTK787, an inhibitor of VEGFR2/kinase insert domain containing eeceptor (KDR), was purchased from MedChemExpress (Princeton, NJ, USA).

2.2. Endometriosis animal model

All animal works were approved by the Animal Experimentation Ethics Committee and performed in accordance with institutional guidelines. All procedures were performed in compliance with relevant laws and institutional guidelines and the appropriate institutional committee approved them. It was conducted in compliance with the local animal ordinance. Eight-week-old C57BL/6 female mice provided by the Laboratory Animal Service Center were housed in a pathogen-free animal house. Anesthesia (100 mg/kg ketamine, 10 mg/kg xylazine in 0.9% saline water) was intraperitoneally injected before surgery. Ovariectomy was performed 7 days before transplantation. 100 μg/kg estradiol-17β (E2; Sigma-Aldrich, St. Louis, MO, USA) was injected via intramuscular at the time of ovariectomy and every 5 days to synchronize the E2 cycle. Endometriotic tissues of the uterine fragments obtained from sacrificed donor mice were cut into 2 mm fragments using a dermal biopsy punch (Miltex, Princeton, NJ, USA). The endometriosis model was established on Day 0 by subcutaneous transplantation of 3 endometrial tissues into the subcutaneous pockets on the abdominal wall of each recipient mouse, as previously described [18]. The subcutaneous model favored longitudinal quantification of the lesion's growth and extended accessibility of microvascular network imaging. Monitoring lesion growth and vessel formation can be thoroughly and efficiently observed using a subcutaneous mouse model. For the prevention experiments, the mice were randomly assigned to one of the following treatments on the day of transplantation: dimethyl sulfoxide (DMSO) in phosphate-buffered saline (PBS) vehicle as a negative control; PTK787 and GnRH agonist (Sigma-Aldrich, St. Louis, MO, USA) as positive controls; and EGCG (50 mg/kg) or ProEGCG (25 mg/kg or 50 mg/kg). The mice were administered with drugs or controls orally for 4 weeks until termination for sample collection. For treatment experiments, the mice were treated with water for 2 weeks and randomly assigned and administered EGCG, ProEGCG, and controls for 4 weeks until termination. For recurrence experiments, the mice were treated on the day of transplantation for 8 weeks, followed by saline water for another 4 weeks. To study the direct binding target in the current study, we employed intraperitoneal injections *in vivo* to compensate for low bioavailability by oral administration. The mice were randomly assigned and administered EGCG (50 mg/kg), ProEGCG (50 mg/kg) or controls. The Animal Experimentation Ethics Committee approved all animal experiments (Approval number: 13-037-MIS). At the end of treatments, lesion area (mm^2) was measured with a digital caliper and calculated under the following formula: length (mm) × width (mm) × π/4. Lesion weight (g) was measured on an electronic balance (Sartorius, Goettingen, Germany).

2.3. Human cell lines

The human endometrial stromal cell line, SHT290, was purchased from Kerafest (Boston, MA, USA). Human endometriotic cell line, HS293 (C). T, was purchased from ATCC (Manassas, VA, USA). The cell culture medium was Dulbecco's modified Eagle medium (DMEM)/nutrient mixture F-12 (Thermo Fisher Scientific Inc., Waltham, MA, USA) with 5% fetal bovine serum (FBS) (Thermo Fisher Scientific Inc.), and 1% anti-anti (Gibco, Waltham, MA, USA).

Cells were passaged every 2–3 days at 80% confluency with TrypLE™ Express Enzyme (Gibco). Cells were grown at 37 °C in an incubator with an atmosphere of >95% humidity and 5% CO_2.

2.4. Cell viability assay

Cell viability assays were performed using Cell Titer-Blue® (Promega, Madison, WI, USA). Cells were placed in 96-well assay plates at a density of 3000 cells per well and incubated at 37 °C with EGCG and ProEGCG in a range of 0–300 μM for 48 h. Cells treated with vehicle or DMSO were used as negative controls, while reagents with no cells were used as blank controls. Twenty microliters per well of Cell Titer-Blue® reagent was added to the cells after 48 h of incubation. The plate was incubated at 37 °C again for 4 h, which was then quantified with fluorescence measurement at 560/590 nm.

2.5. PISA analysis

For 1D PISA assays, SHT290 and HS293 cells were used. HS293 (C). T was cultured and grown to 80% confluence. EGCG and ProEGCG at 4 × IC_{50} concentrations, as well as DMSO, were added to each flask of the cells and incubated for 2 h. Each treatment was performed in triplicate. Cells were harvested in PBS with protease inhibitors (Roche, Basel, Switzerland). The cell solution was split into 15 equal portions in polymerase chain reaction (PCR) tubes. Each portion was thermally treated at a fixed temperature from 43 to 57 °C for 3 min in a SimplyAmp thermal cycler (Applied Biosystems, Waltham, MA, USA). The thermally treated cells were then left at room temperature for 6 min, and lysates were obtained by freeze-thaw cycles 4 times and vortexed briefly after that. All temperature-treated protein precipitates of lysates from the same cell lines were combined. Unfolded proteins were obtained by discarding the pellet after ultracentrifugation sedimentation using an Optima XPN-80 ultracentrifuge (Beckman Coulter, CA, USA). To combine and analyze results from two different cell lines, combined lysates from both cell lines were included and analyzed under the same LC-MS/MS run, along with the treatment and control groups. Cells were lysed using lysis buffer (pH 8.5) composed of 1% sodium dodecyl sulfate, 8 M urea, and 50 mM Tris. The lysates were subjected to thermal treatment as mentioned above.

For 2D PISA analysis, SHT290 and HS293 cells were used. HS293 (C). T was cultured and grown to 80% confluence and lysed by the freeze and thaw method. Cell lysates resuspended in PBS and protease inhibition buffer was treated with different concentrations of EGCG and ProEGCG for 25 min. This was followed by thermal treatments as described above. For the highest drug concentration or control groups, all thermally treated protein precipitates of lysates from the corresponding groups and the same cells were combined, as in the 1D PISA assay. For the remaining tubes from intermediate concentrations, all temperature-treated protein precipitates of lysates of the same cells were combined in one pool. Unfolded proteins were obtained by ultracentrifugation sedimentation as described above. A combined lysate from both cell lines as described was also included.

All samples, including the combined lysates, were processed for proteomics as described previously [19]. In brief, each treatment group underwent protein reduction, alkylation, and digestion. For the combined lysate group, 25 μg of lysate samples from each cell line were combined for further processing as in the other groups. For other groups, 25 μg of each sample was transferred to a new tube for tandem mass tag (TMT) labeling. All labeled samples were desalted and cleaned using C_{18} (Sep-Pak, C_{18}, Vac 1 cm3, 50 mg; Waters, Milford, MA, USA) and underwent high pH reversed-phase fractionation. Twenty-four fractions were collected for LC-MS/MS analysis. For chemical proteomics, each of the fractions was analyzed by nano high-performance liquid chromatography electrospray ionization MS/MS in a Q Exactive HF mass spectrometer (Thermo Fisher Scientific Inc.) under higher-energy collision dissociation. MS/MS spectra were operated in positive ion and data-dependent mode, and MaxQuant v 1.6.2 was used to extract the raw data as well as to identify and quantify the protein. The Andromeda engine was used to match the MS/MS spectra against the complete proteome reference database in Homo sapiens downloaded from UniProt (UP000005640). The datasets of either cell line extracted from MaxQuant were analyzed together or separately for different data analysis purposes. Only proteins with at least two unique peptides were included. The total ion abundance of TMT10 reporters was calculated to normalize the quantification value of every protein, which was then normalized by that of combined lysates, as well as the average abundance of the control groups. The differences between the treated and control groups were finalized.

2.6. Protein-protein interaction (PPI) analysis

String version 11 (https://string-db.org) was used for protein network analysis. Medium confidence with a threshold of 0.4 was used to define the protein-protein network. Default enrichment was performed to show a network around the input. Enrichment analysis with the whole genome as a background dataset was used to identify the enriched terms and pathways.

2.7. In silico molecular analysis

Molecular docking was employed to predict the noncovalent binding of metadherin (MTDH) to EGCG and PX domain containing serine/threonine kinase-like (PXK) to ProEGCG. The pdb structure of MTDH was downloaded from the Protein Data Bank (https://www.rcsb.org), while that of PXK was obtained by performing homology modeling (https://swissmodel.expasy.org). Autodock Tools, version 4.2, and AutoDock Vina version 1.1.2 were used to stimulate the affinity energy of complexes as previously described [18]. Ligplot (https://www.ebi.ac.uk/thornton-srv/software/LIGPLOT/) was used to render the 2D interaction scheme of ligand-protein complexes and identify residues involved in intermolecular interactions as previously described [18]. AutoDock was used to render the 3D interaction scheme of ligand-protein complexes.

2.8. Octet Biorad96e analysis

Recombinant MTDH and PXK (Abcam, Waltham, MA, USA) proteins were immobilized to Octet® Super Streptavidin (SSA) Biosensors (Sartorius) using Octet RED96e (FortéBio, Fremont, CA, USA). For binding kinetics assays, serial dilutions of six concentrations (10, 60, 120, 180, 240, and 300 μM) of EGCG and ProEGCG dissolved in PBS and DMSO were added to a black polypropylene 96-well microplate (Greiner Bio-One, Frickenhausen, Germany) with PBS filling the rest of the wells. An assay cycle consisted of baseline incubation in PBS followed by association in compound solution followed by dissociation in PBS, and it was repeated for every concentration and with both an RBD-loaded and a blank probe. Data were analyzed using Octet Data Analysis HT v.10.

2.9. Human samples

Ectopic and eutopic endometriotic tissue sections were obtained from endometrial biopsies by laparotomic or laparoscopic surgery. Recruited patients were diagnosed with ovarian or peritoneal endometriosis. Control patients were infertile women

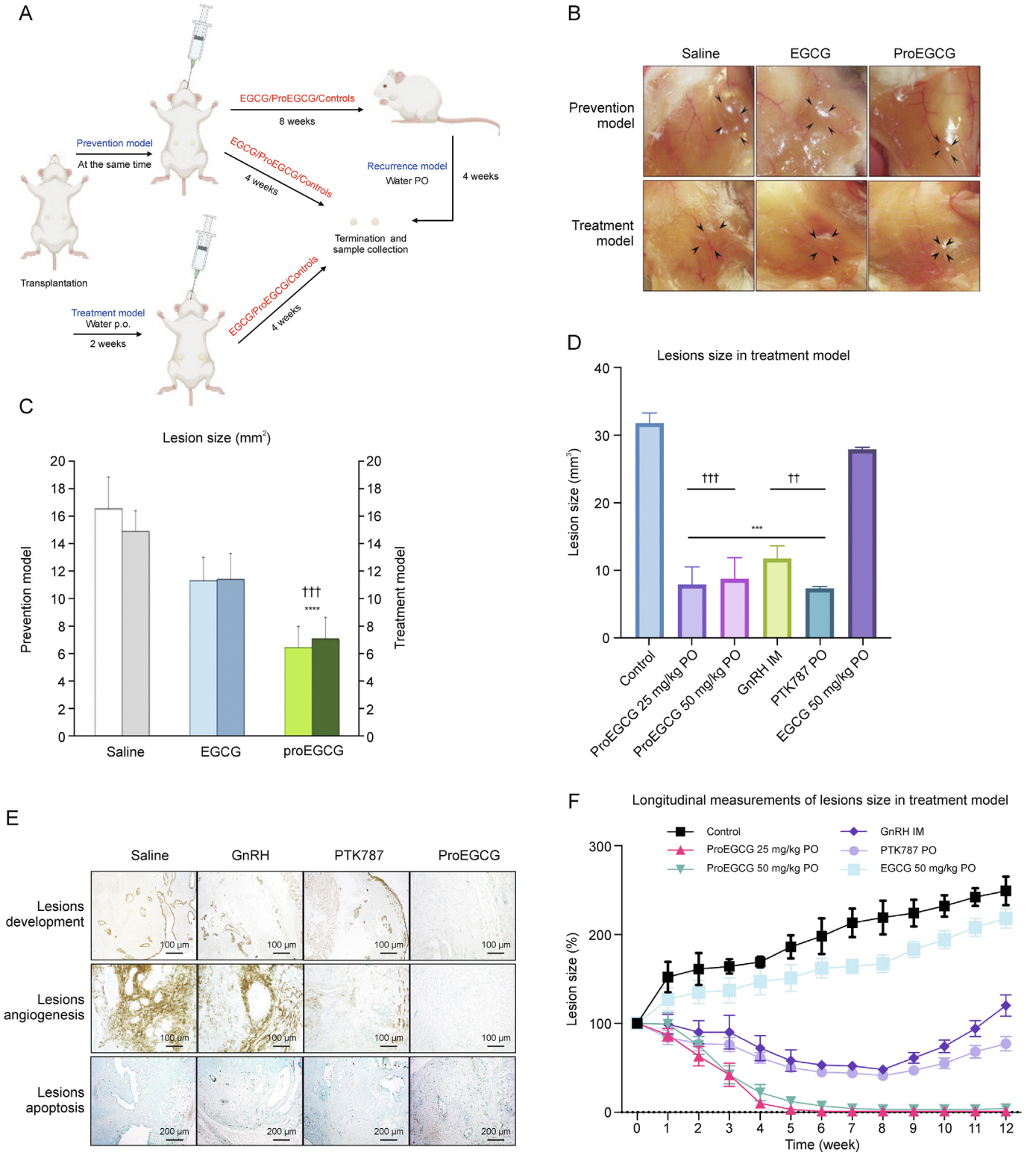

Fig. 1. The efficacy of *epigallocatechin* gallate (EGCG) and prodrug of *epigallocatechin* gallate (ProEGCG) as a therapeutic or preventive medicine. (A) Schematic diagram of the prevention, treatment, and recurrence endometriosis mice models to investigate the efficacy of EGCG and ProEGCG. (B) Representative images to show the endometriotic lesions after different treatments in prevention and treatment models. (C) Bar chart to show the lesions size changes after EGCG (50 mg/kg) or ProEGCG (25 mg/kg or 50 mg/kg) treatment in prevention and treatment model. Data showed mean ± standard error of mean (SEM). $^{****}P < 0.0001$, compared to control; $^{\dagger\dagger\dagger}P<0.001$, compared to EGCG groups in either prevention or treatment model. (D) Lesions size after 8 weeks under different treatments in treatment model. Data showed mean ± SEM ($n = 3$). $^{***}P < 0.001$, compared to control; $^{\dagger\dagger}P < 0.01$, $^{\dagger\dagger\dagger}P < 0.001$, compared to EGCG 50mg/kg PO group. (E) Histology images to show lesions development, angiogenesis, and apoptosis under different treatments for 8 weeks in treatment model. These are assessed by keratin, CD31 and terminal deoxynucleotidyl transferase-mediated deoxyuridine triphosphate-nick end labelling (TUNEL) markers. (F) Longitudinal measurement of the lesions sizes percentage changes were recorded every week under different treatments. During weeks 8–12, the mice were administered with saline water to observe the recurrence of lesions. Data showed mean ± SEM ($n = 3$). $^{***}P < 0.001$, $^{****}P < 0.0001$, compared to control. PO: oral administration; IM: intramuscular injection; GnRH: gonadotropin-releasing hormone.

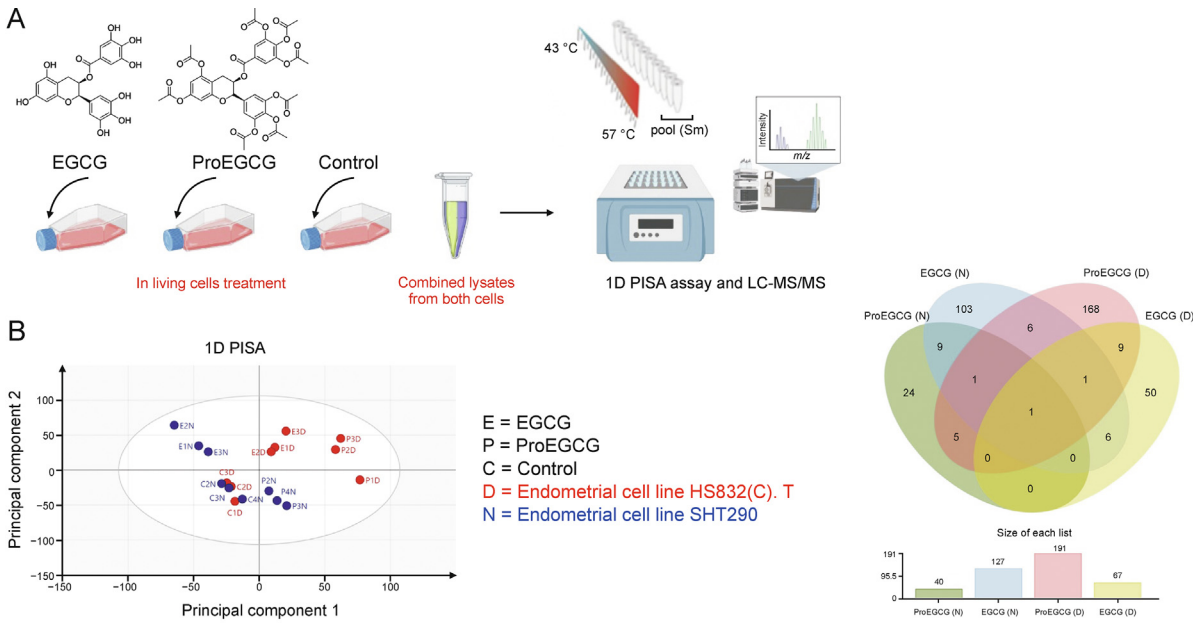
A
EGCG
ProEGCG
Control
In living cells treatment
Combined lysates from both cells
43 °C
57 °C
pool (Sm)
Intensity
m/z
1D PISA assay and LC-MS/MS
B
1D PISA
Principal component 2
Principal component 1
E = EGCG
P = ProEGCG
C = Control
D = Endometrial cell line HS832(C). T
N = Endometrial cell line SHT290
EGCG (N)
ProEGCG (D)
ProEGCG (N)
EGCG (D)
Size of each list
C
ProEGCG vs EGCG in SHT290
ΔSm ProEGCG
ΔSm EGCG
$P_{EGCG, PROEGCG} \leq 0.05$
$R^2 = 0.2992$
$n_{\Delta Sm > 0.5 \text{ or } < -0.5} = 11$
Blood vessel morphogenesis
Protein complex oligomerization
Cellular response to transforming growth factor beta stimulus
Regulation of mRNA processing
ProEGCG vs EGCG in HS832(C). T
$P_{EGCG, PROEGCG} \leq 0.05$
$R^2 = 0.5036$
$n_{\Delta Sm > 0.5 \text{ or } < -0.5} = 10$
Cellular component organization
Mitochondrial electron transport
Oxidation-reduction process
Mitochondrion organization
D
EGCG on HS832(C).T vs SHT290
ΔSm Hs832(C).T
ΔSm SHT290
$P_{d.n} \leq 0.05$
$R^2 = 0.4693$
$n_{\Delta Sm > 0.5 \text{ or } < -0.5} = 8$
Cellular response to organic substante
Blood vessel development
Carboxylic acid metabolic process
Cellular response to oxygen-containing compound
Cellular response to transforming growth factor beta stimulus
ProEGCG on HS832(C).T vs SHT290
$P_{d.n} \leq 0.05$
$R^2 = 0.4116$
$n_{\Delta Sm > 0.5 \text{ or } < -0.5} = 7$
Macromolecule metabolic process
Cellular component organization

without endometriosis. All procedures were performed in compliance with relevant laws and institutional guidelines and the appropriate institutional committee approved them. It is approved by the Hospital Authority of Hong Kong and The Chinese University of Hong Kong (Approval number: 2013.202). All patients provided informed written consent for tissue collection for research purposes.

2.10. Immunohistochemistry (IHC) analysis

Lesion tissues from humans and mice were fixed in 10% buffered formalin for 24 h, embedded in paraffin blocks and cut into slices of 4 μm thickness. Sections were deparaffinized and incubated with 3% hydrogen peroxide in the dark to block endogenous peroxidase activity. The sections were then incubated in boiled 10 mM sodium citrate buffer, pH 6, for antigen retrieval and boiled in a conventional microwave for 2 min 2 times. The sections were cooled, followed by blocking with 5% goat serum in 1% bovine serum albumin (BSA)/PBS and goat F(ab) anti-mouse IgG H&L (ab6668, Abcam) to reduce nonspecific signal and nonspecific binding of the mouse serum to mouse tissue. The tissues were then incubated with primary antibodies overnight, followed by secondary antibodies for 1 h and developed in 3,3-diaminobenzidine for 3–5 min. After mounting, a Leica DM6000B microscope (Leica, Witzler, Germany) was used for image capture. For semiquantitative analysis, protein expression was quantified by H-score using Qupath v0.3.1 (https://qupath.github.io), as calculated by summing up the percentage of different intensity level-stained cells: strongly stained cells (3+), moderately stained cells (2+), weakly stained cells (1+) and unstained cells (0) of a fixed field. H-score = [1 × (% 1+)+2 × (%2+)+3 × (%3+)]. Each field was selected randomly and repeated to capture five fields. The final cell count was reported as the average of the five fields.

2.11. RNA extraction

Lesions were collected in RNAlater solution at 4 °C and incubated for 24 h, followed by removal of the supernatant, and the tissues were stored at −80 °C for long-term storage. Total RNA was extracted by the RNeasy mini kit (Qiagen, Hilden, Germany) and assessed with Nanodrop ND-2000 spectrophotometers (Thermo Fisher Scientific Inc.). For all RNAs, the 260/280 ratio was ~2.

2.12. Microarray analysis

Whole genome expression microarray analysis of mice ($n = 3$ per treatment group) was performed and analyzed according to previous procedures using GeneSpring GX 11.0 software (Agilent Technologies, Santa Clara, California, USA) Cluster 3.0 (http://bonsai.hgc.jp/~mdehoon/software/cluster/software.html) and Java Treeview (http://jtreeview.sourceforge.net) [14–16,18].

2.13. PCR analysis

To assess the gene expression level changes of *PXK*, *MTDH*, and downstream proteins after treatments, RNA was extracted for reverse transcription and quantitative real-time reverse transcription polymerase chain reaction assay (qRT-PCR). TB Green Premix Ex Taq (Tli RNaseH Plus) (Takara, Shiga, Japan) was used to amplify the gene expression and quantified by a LightCycler 480 quantitative PCR system (Roche). Human alpha-tubulin or mouse *Gapdh* genes were used as housekeeping genes to normalize the gene expression of the studied proteins. PCR primers for all examined genes are listed in Tables S1 and Table S2.

2.14. Cell transfection assay

Small interfering RNA (siRNA) transfection was performed with si-PXK (Human) and si-MTDH (Human) (Horizon, Cambridge, United Kingdom) and negative control siRNA. One day before transfection, cells were equally placed in 6-well plates at a confluency of 40%–50% and incubated at 37 °C overnight. The medium was changed to an antibiotic-free medium. On the day of transfection, Opti-MEM I reduced serum medium (Gibco) was incubated with Lipofectamine 2000 transfection reagent (Invitrogen, Waltham, MA, USA) and siRNA at room temperature for 20 min. The final concentrations of siRNAs were 20 nM or 50 nM. The mixture was then added to the cells and incubated for 24 h.

2.15. Knockdown mouse models

siRNA local administration through microneedle was employed as previously described [20]. Topical injection of siRNA was effectively delivered into the lesions and inhibited lesion progression. An endometriosis model was established by subcutaneous transplantation of two lesions as described above. Mice were rested for 2 weeks after transplantation and before siRNA treatments to allow lesion growth. The mice were then randomly assigned to one of the following treatments for one week: Pxk-siRNA, Mtdh-siRNA, and siRNA negative control groups (Abbexa, Cambridge, UK).

2.16. Cellvizio analysis

Microvascular network imaging of the lesions was monitored by a Cellvizio 488 system with a ProFlex Microprobe S100 (Mauna Kea Technologies, Paris, France). Then, 75 mg/kg fluorescein isothiocyanate (FITC)-labeled dextran (Sigma-Aldrich, St. Louis, MO, USA) was injected via the intraorbital vein. After a few minutes of injection, the appearance of microvessels in the lesions was assessed and visualized by fiber confocal fluorescence. The optical mini probe was operated in manual mode. Angiotools version 0.5 (https://angiotool.software.informer.com/0.5/) was used to quantitatively assess the vessel percentage area and density. The system was set to only detect vessels with diameters of 10 μm, 15 μm, and 20 μm, and foreground and background small particles were removed.

Fig. 2. The differential binding targets of *epigallocatechin* gallate (EGCG) and prodrug of *epigallocatechin* gallate (ProEGCG) on a proteome wide scale. (A) 1D proteome integral solubility alteration (PISA) proteomics approach to differentiate protein targets of EGCG and ProEGCG in living cells ($n = 3$). (B) (Left) Principal components analysis (PCA) plot of results from 1D PISA. (Right) Venn diagram and bar chart to show numbers of intersecting protein targets of EGCG or ProEGCG in SHT290 (N) or HS832(C). T. (D) cells line in 1D PISA. Only proteins with $P < 0.05$ and ΔSm >0.05 or < −0.05 were included. (C) (Upper panel) 1D PISA analysis on SHT290 endometrial stromal cells (left) and HS832(C). T endometriotic cell lines (right). Correlation plot for EGCG vs ProEGCG treatment in either cell. Proteins with $P < 0.05$ across the two parameters were shown only. (Lower panel) String network connected proteins that bind to both EGCG and ProEGCG in SHT290 endometrial stromal cells (left) or HS832(C). T endometriotic cell lines (right). String network connected proteins that bind to EGCG (left) or ProEGCG (right) in both cells. Pathway enrichment was increased by adding 5 extra nodes. Predicted associations between proteins were shown by edges. The nodes represented the proteins and colors denoted the selected biological processes the proteins were responsible for. These analyses were done by gene ontology functional enrichment. (D) (Upper panel) 1D PISA analysis on EGCG (left) and ProEGCG (right) protein targets across two cell lines. Correlation plot of EGCG or ProEGCG on HS832(C). T. endometriotic cells vs SHT290 endometrial stromal cells. Proteins with $P < 0.05$ across the two parameters were shown only. R^2 denoted the correlation coefficient. (Lower panel) String network connected proteins that bind to EGCG (left) or ProEGCG (right) in both cells. LC-MS/MS: liquid chromatography with tandem mass spectrometry; ΔSm: difference in abundance.

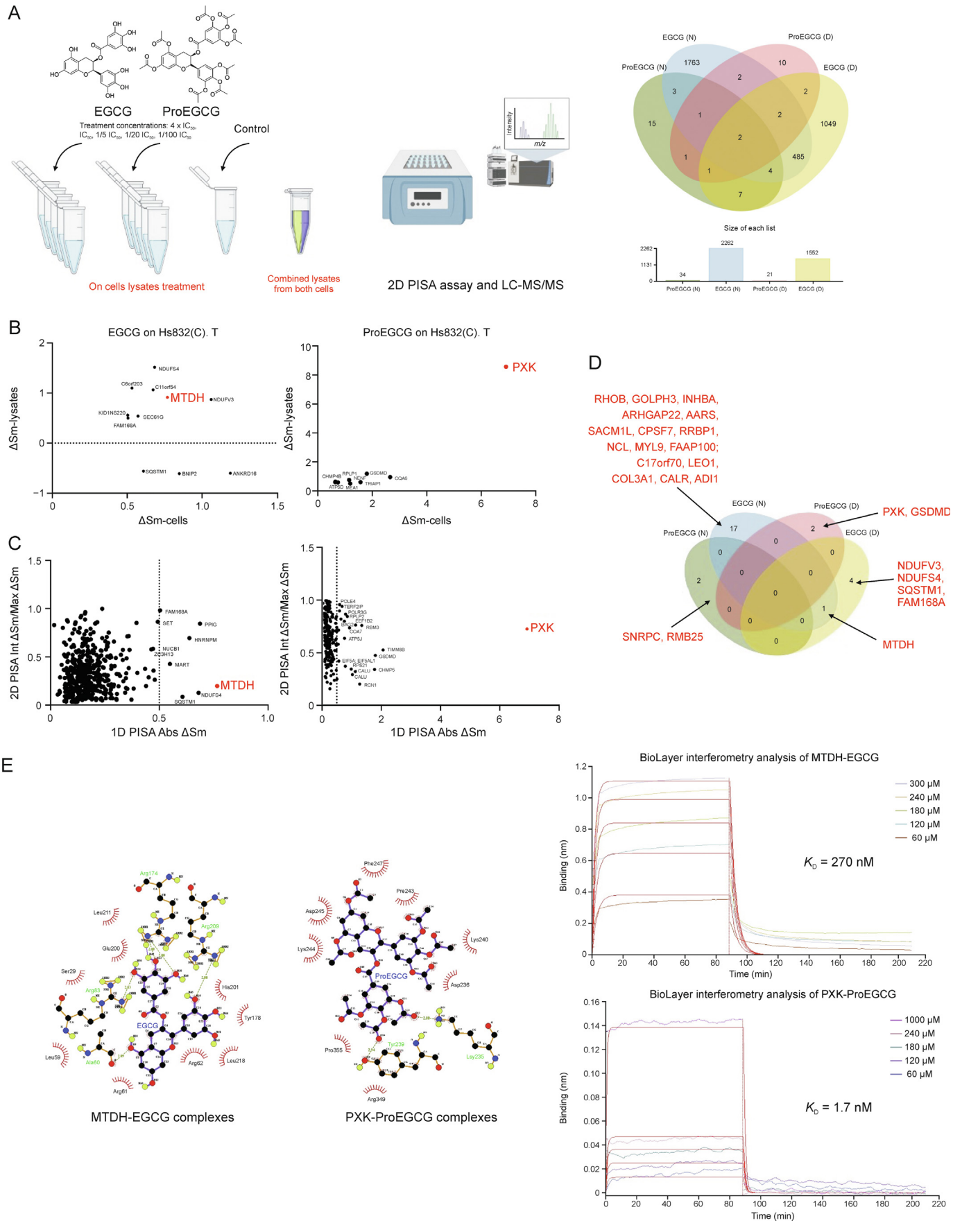
A
EGCG
ProEGCG
Treatment concentrations: 4 x IC50, IC50, 1/5 IC50, 1/20 IC50, 1/100 IC50
Control
On cells lysates treatment
Combined lysates from both cells
2D PISA assay and LC-MS/MS
EGCG (N)
ProEGCG (D)
ProEGCG (N)
EGCG (D)
Size of each list
ProEGCG (N)
EGCG (N)
ProEGCG (D)
EGCG (D)
B
EGCG on Hs832(C). T
ProEGCG on Hs832(C). T
ΔSm-lysates
ΔSm-cells
MTDH
PXK
C
2D PISA Int ΔSm/Max ΔSm
1D PISA Abs ΔSm
MTDH
PXK
D
RHOB, GOLPH3, INHBA, ARHGAP22, AARS, SACM1L, CPSF7, RRBP1, NCL, MYL9, FAAP100; C17orf70, LEO1, COL3A1, CALR, ADI1
PXK, GSDMD
NDUFV3, NDUFS4, SQSTM1, FAM168A
SNRPC, RMB25
MTDH
E
MTDH-EGCG complexes
PXK-ProEGCG complexes
BioLayer interferometry analysis of MTDH-EGCG
300 μM
240 μM
180 μM
120 μM
60 μM
K_D = 270 nM
Binding (nm)
Time (min)
BioLayer interferometry analysis of PXK-ProEGCG
1000 μM
240 μM
180 μM
120 μM
60 μM
K_D = 1.7 nM
Binding (nm)
Time (min)

2.17. Enzyme-linked immunosorbent assay (ELISA) analysis

The mouse 17β-estradiol (ab108667, Abcam) and progesterone (ab285257, Abcam) ELISA kits were purchased. Human VEGFA ELISA kit (ab119566, Abcam) and Human HIF-1 alpha ELISA kit (ab171577, Abcam) were used to test the vascular endothelial growth factor A (VEGFA) and hypoxia-inducible factor (HIF) 1α protein levels of medium and lysates extracted from HS293 (C). T cells. Standards and samples were added to antibody-coated test wells, followed by an antibody cocktail, according to the manufacturer's guidance. The wavelengths of the different ELISA kits were as follows: 17β-estradiol ELISA kit ab108667: 450 nm; progesterone ELISA kit ab285257: 405 nm; Human VEGFA ELISA kit ab119566: 450 nm; Human HIF-1 alpha ELISA kit ab171577: 450 nm. Absorbance measurements were recorded.

2.18. Statistical analysis

For the chemical proteomics analysis, the F test followed by two-tailed Student's *t*-test was used to obtain the *P* value. Volcano and correlation plots were prepared using Prism. Multivariate variable pattern recognition of the whole set of proteomes was performed using SIMCA® version 15.0.2 with the default setting for regression analysis of discrete variables. For other *in vitro* and *in vivo* assays, one-way analysis of variance (ANOVA) was used for comparisons of more than two groups. Tukey's post hoc test was used for multiple comparisons. For comparison between just two groups, an unpaired Student's *t*-test was used. All statistical analyses were performed by Prism. $P \leq 0.05$ was considered statistically significant. Standard derivation was used as a representation of the error range.

3. Results

3.1. ProEGCG as an effective preventive and treatment regimen for endometriosis

Prevention and treatment endometriosis mouse models were established (Figs. 1A and B), in which EGCG (50 mg/kg) and ProEGCG (25 mg/kg and 50 mg/kg) were administered to mice orally. ProEGCG possessed stronger inhibitory effects on lesion growth than EGCG in both models (Fig. 1C). ProEGCG treatment (25 mg/kg) was shown to be the best regimen, which inhibited 80% of the endometriotic lesion size compared to controls (Fig. 1D). ProEGCG demonstrated the greatest potency to inhibit lesion growth, increase apoptosis in lesions, downregulate angiogenic marker CD31 (Fig. 1E), and prevent lesion recurrence, as seen in PTK787 and GnRH (Fig. 1F). ProEGCG did not affect body weight or dysregulated endogenous female hormones, including estrogen and progesterone levels (Fig. S1).

3.2. MTDH and PXK as the binding targets of EGCG and ProEGCG, respectively

A 1D PISA assay was used to study cellular target engagement and identify protein targets of EGCG and ProEGCG in SHT290 and HS832 (C) cells in the cell lines regardless of whether the drugs were metabolized (Figs. 2A and S2–S4). The principal components analysis (PCA) plot showed distinct clusters of EGCG or ProEGCG treatment on either endometrial or endometriotic cells (Fig. 2B). EGCG (N = 127, D = 67) had a similar number of targets as ProEGCG (N = 40, D = 191) (Fig. 2B). Fig. 2C shows differential targets of drugs in the same cells. EGCG and ProEGCG were significantly more correlated in endometriotic cells ($R^2 = 0.5036$, $P \leq 0.05$) than in endometrial cells ($R^2 = 0.2992$, $P \leq 0.05$). Fig. 2D shows differential targets of drugs in different cells. Both EGCG ($R^2 = 0.4693$, $P \leq 0.05$) and ProEGCG ($R^2 = 0.4116$, $P \leq 0.05$) had correlated drug targets on endometriotic cells against endometrial cells. ΔSm denotes the difference in abundance between the drug-treated and control groups. The most prominent and significant binding proteins (ΔSm value of >0.5 or < −0.5) were connected by the String PPI network to further explain the mutual or differential involvement of EGCG and ProEGCG in the same or different cells.

2D PISA analysis was used to study the direct ligand-target engagement and confirm the protein targets of EGCG and ProEGCG in their original form on cell lysates, depending on the treatment concentration (Figs. 3A and S5–S7). Lysate treatment of ProEGCG (N = 34, D = 21) resulted in fewer targets than that of EGCG (N = 2262, D = 1552), owing to the bulky chemical structure of ProEGCG. Protein targets of drugs at maximum concentrations in cells or on cell lysate treatments were correlated (Figs. 3B and S8). EGCG treatment had little correlation in both endometrial ($R^2 = 0.01457$) and endometriotic cells ($R^2 = 0.01076$), while ProEGCG treatment had more correlation in both endometrial cells ($R^2 = 0.1895$) and endometriotic cells ($R^2 = 0.5808$). Corresponding scatter plots of absolute ΔSm (1D PISA assay) against Int ΔSm/Max ΔSm (2D PISA) were constructed and showed that the most putative targets were concentration dependent (Figs. 3C and S9). These included RHOB, INHBA, GOLPH3, and COL3A1 as targets of EGCG, and RBM25 and SNRPC as targets of ProEGCG in endometrial stromal cells; MTDH, NDUFS4, SQSTM1, FAM168A, and NDUFV3 as targets of EGCG; and PXK and GSDMD as targets of ProEGCG in endometriotic cells (Fig. 3D). Among all, MTDH and PXK were the most significant and strongest binding targets of EGCG and ProEGCG, respectively, in both endometriotic cells and lysates. MTDH resulted in ΔSm values of 0.77 (−log10(*P* value): 4.33) and 0.92 (−log10(*P* value): 4.33) by binding to EGCG from 1D and 2D PISA, respectively, while PXK resulted in ΔSm values of 6.92 (−log10(*P* value): 2.18) and 8.57 (−log10(*P* value): 1.81) by binding to ProEGCG from 1D and 2D PISA, respectively.

Fig. 3. The novel and direct binding targets of *epigallocatechin* gallate (EGCG) and prodrug of *epigallocatechin* gallate (ProEGCG). (A) (Left) 2D proteome integral solubility alteration (PISA) proteomics approach to differentiate protein targets of EGCG and ProEGCG in cell lysates ($n = 3$). (Right) Venn diagram and bar chart to show the numbers of intersecting protein targets of EGCG or ProEGCG under maximum concentration in SHT290 or HS832(C). T cells line in 2D PISA. Only proteins with $P < 0.05$ and ΔSm >0.05 or < −0.05 were included. (B) Overall plot to show EGCG (left) and ProEGCG (right) under maximum concentration treatments in HS832(C). T. endometriotic stromal cells. Correlation plots (ΔSm (lysates) vs ΔSm (in cells)) to correlate 1D and 2D PISA. Proteins with $P < 0.05$ and ΔSm > 0.5 or < −0.5 in both across the two parameters were shown only. (C) Scatter plots of absolute value of ΔSm in cells from 1D PISA vs absolute value of (Int ΔSm/Max ΔSm) in cell lysates from 2D PISA, Proteins with $P < 0.05$ across all parameters (maximum concentration treatment in cells and on lysates, as well as intermediate concentration treatment on lysates) were shown only. Red dotes denoted metadherin (MTDH) or PX domain containing serine/threonine kinase-like (PXK). (D) Venn diagram to show protein targets of EGCG or ProEGCG in SHT290 and HS832(C). T cells line incorporating 1D and 2D PISA datasets. Only proteins with $P < 0.05$ and ΔSm > 0.05 or < −0.05 and dependent to concentration of drugs were included (Int ΔSm/Max ΔSm ≤ 1). (E) (Left) Ligplot shows the interaction analysis of structures of protein-ligands binding sites of MTDH-EGCG and PXK-ProEGCG in a 2D interaction scheme are shown. (Right) Biolayer interferometry (BLI) binding studies and binding kinetics were measured with the Octet RED96 instrument (ForteBio, Pall Corporation, Portland, NY, USA). Biotinylated MTDH and PXK were immobilized on super streptavidin (SSA) biosensor tips and incubated over a range of concentrations (10, 60, 120, 180, 240, 300, and 1000 μM) of EGCG or ProEGCG. Data was fit globally to different binding schemes corresponding to a 1:1 binding isotherm. Fitted equilibrium binding constants are shown. LC-MS/MS: liquid Chromatography with tandem mass spectrometry; ΔSm: difference in abundance; K_D: dissociation constant.

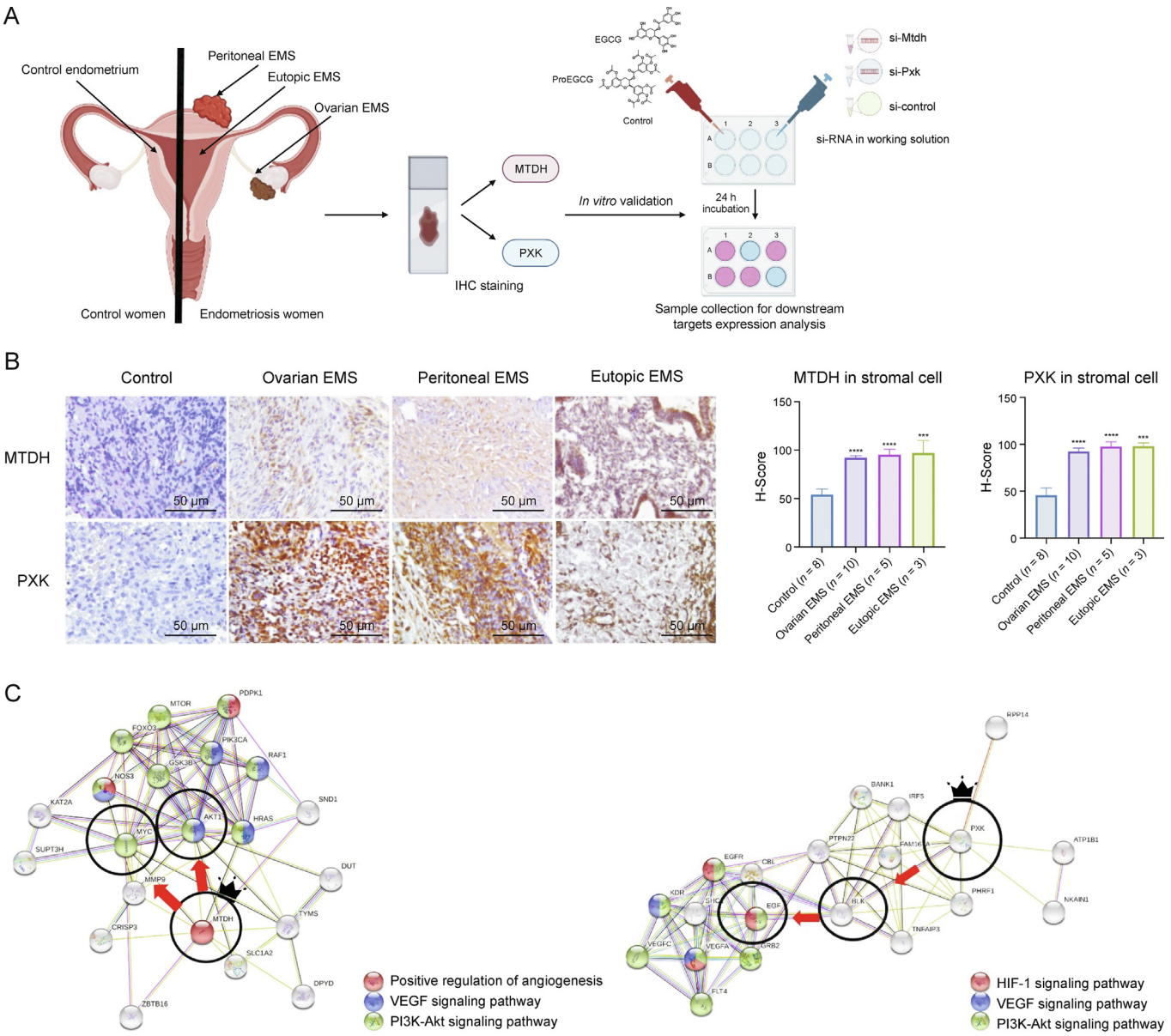
A
Control endometrium
Peritoneal EMS
Eutopic EMS
Ovarian EMS
Control women
Endometriosis women
MTDH
PXK
IHC staining
EGCG
ProEGCG
Control
si-Mtdh
si-Pxk
si-control
si-RNA in working solution
In vitro validation
24 h incubation
Sample collection for downstream targets expression analysis
B
Control
Ovarian EMS
Peritoneal EMS
Eutopic EMS
MTDH
PXK
50 μm
MTDH in stromal cell
PXK in stromal cell
H-Score
Control (n = 8)
Ovarian EMS (n = 10)
Peritoneal EMS (n = 5)
Eutopic EMS (n = 3)
C
Positive regulation of angiogenesis
VEGF signaling pathway
PI3K-Akt signaling pathway
HIF-1 signaling pathway
VEGF signaling pathway
PI3K-Akt signaling pathway
D
Gene expression levels of EGCG targets in HS832 (C). T.
Gene expression levels of ProEGCG targets in HS832 (C). T.
Fold change relative to control (gene/AT expression ratio)
MTDH
MYC
Akt
PXK
BLK
EGF
Control
EGCG 3*IC50
EGCG 4*IC50
ProEGCG 3*IC50
ProEGCG 4*IC50
E
Gene expression levels of EGCG targets in HS832 (C). T.
Gene expression levels of ProEGCG targets in HS832 (C). T.
Fold change relative to control (gene/AT expression ratio)
MTDH
MYC
Akt
PXK
BLK
EGF
Control
si-MTDH 20 nM
si-MTDH 50 nM
si-PXK 20 nM
si-PXK 50 nM

3.3. Direct binding of MTDH-EGCG and PXK-ProEGCG complexes

The 2D and 3D interaction schemes of the MTDH- and PXK-ligand complexes showed the amino acids involved in the binding pockets (Figs. 3E, S10, and S11, and Table S3). Five hydrogen bonds (Ala 60, Arg 83, Arg 174, Arg 174, and Arg 209) and 9 hydrophobic interactions were formed between MTDH and EGCG (affinity energy of −7.9 kcal/mol). Two hydrogen bonds (Lys 235 and Lys 239) and 8 hydrophobic interactions were formed between PXK and ProEGCG (affinity energy of −6.8 kcal/mol).

The association and dissociation constants of the 2 targets to drug binding were evaluated using biolayer interferometry (BLI) with an Octet RED96e system for confirmation. The equilibrium constants (K_D) of MTDH-EGCG and PXK-ProEGCG were 270 nM and 1.7 mM, respectively (Fig. 3E). K_D values of MTDH-ProEGCG and EGCG-PXK were 517 μM and 2.42 mM, respectively (Table S3 and Fig. S12). Both computation stimulation of affinity energy and BLI analysis of kinetic affinity confirmed the strongest complex of MTDH-EGCG and PXK-ProEGCG, while EGCG-PXK and ProEGCG-MTDH were weaker.

3.4. MTDH and PXK are highly expressed in endometriosis

PXK and MTDH protein expression in ectopic and eutopic stromal cells from women with endometriosis was investigated (Fig. 4A). Both MTDH and PXK were significantly overexpressed in ectopic tissues of ovarian and peritoneal endometriosis, as well as eutopic tissues of endometriosis, compared to that from control women without endometriosis (Fig. 4B).

3.5. Signaling pathways of EGCG and ProEGCG in vitro

Gene ontology functional enrichment analyses of MTDH and PXK were examined. MTDH and its associated proteins are involved in the regulation of angiogenesis, particularly in the VEGF and PI3K-Akt signaling pathways (Fig. 4C). Protein kinase B (Akt1) and Myc proto-oncogene protein (MYC) are two proximal downstream targets of MTDH. PXK and its associated proteins were also involved in the angiogenic VEGF, PI3K-Akt and HIF-1a signaling pathways. B lymphocyte kinas (BLK) and epidermal growth factor(EGF) are two proximal downstream targets of PXK. The regulatory effects of EGCG and ProEGCG on PXK and MTDH, as well as their associated downstream genes in endometriotic cells, were confirmed by qRT-PCR (Fig. 4D). PXK and MTDH knockdown cell models confirmed the regulatory effects (Fig. 4E). MTDH and PXK expression was effectively downregulated after si-MTDH and si-PXK transfection, respectively.

For the MTDH signaling network, the gene expression of *Mtdh* was significantly downregulated by high concentrations of EGCG. Gene expression of *MYC* and *Akt1* was significantly downregulated by EGCG or si-MTDH transfection in a concentration-dependent manner. On the other hand, ProEGCG significantly downregulated the gene expression of *MTDH*, *MYC* and *Akt1* in a concentration-dependent manner and delivered greater efficacy than EGCG (Fig. S13A). However, *MYC* and *Akt1* were not downregulated by si-PXK transfection (Fig. S13B).

For the PXK signaling network, the gene expression of *PXK* was significantly downregulated by high concentrations of ProEGCG. Gene expression of *BLK* was also downregulated by ProEGCG or Si-PXK transfection. However, the inhibitory effect was reduced at higher concentrations of ProEGCG, and that of si-PXK did not reach statistical significance. Gene expression of *EGF* was significantly downregulated by ProEGCG at low concentrations or si-PXK transfection. On the other hand, EGCG significantly downregulated the gene expression of *BLK* and *EGF* but had no effect on *Pxk*. Its inhibitory effect on *BLK* was reduced at higher concentrations, while its effect on EGF was significantly weaker than that of ProEGCG. si-MTDH transfection only significantly downregulated *EGF* gene expression, but it had no effect on *PXK* or *BLK* expression levels.

3.6. Signaling pathways of EGCG and ProEGCG in vivo

Downstream signaling pathways of MTDH and PXK in the endometriosis mouse model after treatment with EGCG and ProEGCG were determined by whole transcriptome microarray (Fig. 5A and Table S4). For MTDH signaling (Figs. 5A and B, and Table S4), Total mRNA and protein expressions of *Mtdh* and *Akt* in the lesion stromal cells were significantly downregulated by either EGCG or ProEGCG. The inhibitory effect of ProEGCG on *Akt1* was stronger and more significant than that of EGCG. For PXK signaling, mRNA and protein expression of *Pxk* and *Egf* were downregulated by ProEGCG. EGCG also downregulated the protein expression of *Egf*, but the inhibitory capacity of ProEGCG on *Egf* was more prominent.

To confirm the downstream effects, both *Mtdh* and *Pxk* knockdown mouse models were established (Figs. 5C and Table S5). si-*Pxk* was more effective than si-*Mtdh* in reducing the lesion size. *Mtdh* and *Akt1* mRNA and protein expression levels were downregulated by si-*Mtdh*. *Pxk* and *Egf* mRNA and protein expression levels were downregulated by si-*Pxk* (Fig. 5D and Table S2). These results confirmed the downregulating effects and interactions between *Mtdh* and *Akt1*, as well as between *Pxk* and *Egf in vivo*.

3.7. Antiangiogenic mechanism of MTDH-EGCG and PXK-ProEGCG

In the endometriotic cell line *in vitro* (Figs. 6A and B), the mRNA expression and protein levels of VEGF were significantly downregulated by ProEGCG in a concentration-dependent manner. EGCG only significantly downregulated VEGF protein levels. In the siRNA transfection models, the mRNA expression level of VEGF was also downregulated when either MTDH or PXK was knocked down, but its protein level was only downregulated when PXK was knocked down.

The mRNA expression and protein levels of HIF-1α were significantly downregulated by either EGCG or ProEGCG in a

Fig. 4. Binding targets of *epigallocatechin* gallate (EGCG) and prodrug of *epigallocatechin* gallate (ProEGCG) *in vitro*. (A) Schematic diagram to show the endometriosis subtypes tissues and flow chart of *in vitro* validation. (B) (Left) Representative images of immunohistochemistry (IHC) staining to determine protein expressions of metadherin (MTDH) and PX domain containing serine/threonine kinase-like (PXK) in different subtypes of endometriosis tissues. (Right) IHC scoring system (H-Score) values in normal or diseased endometrial stromal cells. Data showed mean ± standard error of mean (SEM). (C) Enriched protein–protein interaction (PPI) network of MTDH and PXK functional annotations were included. The nodes represented the proteins and colors denoted the selected functions of the proteins. The edges represented the association between proteins. MTDH was labeled with crown icons on top of the nodes. (D) Fold change of binding and downstream targets of EGCG (left) or ProEGCG (right) gene expression levels in HS832 (C). T. cell line after different treatments. Gene levels were normalized relative to housekeeping genes and control. Data show mean ± SEM ($n = 3$). (E) Fold change of binding and downstream targets of EGCG or ProEGCG gene expression levels after transfection with MTDH (left) or PXK (right) siRNA at different concentrations in HS832 (C). T. cell lines. Data show mean ± SEM ($n = 4$). One-way analysis of variance (ANOVA) with Tukey post-hoc test was used for the multiple groups' comparison. $^{*}P < 0.05$, $^{**}P < 0.01$, $^{***}P < 0.001$, $^{****}P < 0.0001$, compared to control; $^{\#}P < 0.05$, $^{\#\#}P < 0.01$, $^{\#\#\#}P < 0.001$, $^{\#\#\#\#}P < 0.001$, compared to the same treatment at the lowest concentration. AT: Alpha tubulin (housekeeping gene). EMS: endometriosis; VEGF: vascular endothelial growth factor; PI3K: phosphoinositide 3-kinase; Akt: protein kinase B; HIF: hypoxia-inducible factor; BLK:tyrosine-protein kinase; EGF: epidermal growth factor; MYC: myc proto-oncogene protein.

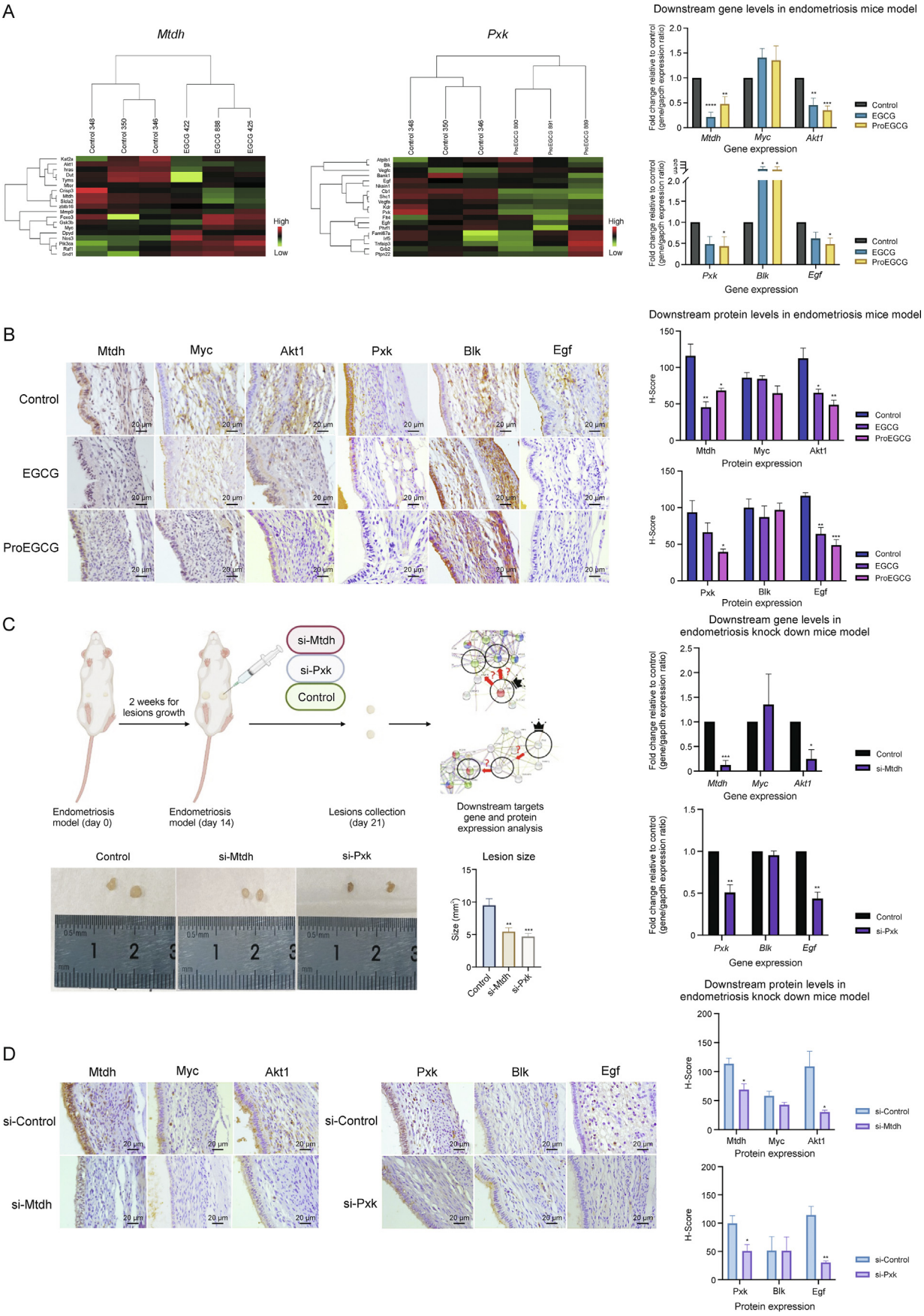
A
Mtdh
Pxk
Control 348
Control 350
Control 346
EGCG 422
EGCG 888
EGCG 425
ProEGCG 890
ProEGCG 891
ProEGCG 889
High
Low
Downstream gene levels in endometriosis mice model
Fold change relative to control (gene/gapdh expression ratio)
Mtdh
Myc
Akt1
Pxk
Blk
Egf
Gene expression
Control
EGCG
ProEGCG
B
Mtdh
Myc
Akt1
Pxk
Blk
Egf
Control
EGCG
ProEGCG
20 μm
Downstream protein levels in endometriosis mice model
H-Score
Protein expression
C
si-Mtdh
si-Pxk
Control
2 weeks for lesions growth
Endometriosis model (day 0)
Endometriosis model (day 14)
Lesions collection (day 21)
Downstream targets gene and protein expression analysis
Lesion size
Size (mm²)
Downstream gene levels in endometriosis knock down mice model
Downstream protein levels in endometriosis knock down mice model
D
si-Control
si-Mtdh
si-Pxk

concentration-dependent manner, while ProEGCG exerted a significantly greater inhibitory effect. HIF-1α gene or protein levels were both downregulated when either MTDH or PXK was knocked down. The inhibitory effects of si-PXK transfection on HIF-1α expression levels were greater than those of si-MTDH transfection.

To investigate the anti-angiogenesis effects *in vivo*, we performed microvascular network imaging (Fig. 6C). The EGCG and ProEGCG treatment groups, as well as the si-*Pxk* and si-*Mtdh* knockdown models, showed reduced vessel percentage area and total number of vessel junctions in the endometriotic lesions. Whole lesion cell total mRNA expression of *Vegfa* and *Hif-1α* (Fig. 6D) was downregulated by EGCG or ProEGCG. Only si-*Pxk*, but not si-*Mtdh*, downregulated *Hif-1α* mRNA expression levels. The protein expression levels of *Vegfa* in lesion stromal cells were significantly downregulated in all treatment groups, and those of *Hif-1a* were only significantly downregulated in the ProEGCG and Si-*Pxk* groups. These results suggested that both EGCG and ProEGCG regulated *Vegfa* and *Hif-1α,* but *Pxk* mediated the anti-angiogenesis effects more strongly than *Mtdh*.

4. Discussion

EGCG is a polyphenolic compound and a well-known antioxidant. It has multiple targets with multiple effects on various signaling pathways, which may potentially regulate the complex pathophysiology of endometriosis [7]. EGCG exerts antiangiogenic effects via the VEGFC/VEGFR2 pathways, antioxidant effects via a reactive oxygen species scavenging mechanism, and anti-proliferative effects via a reduction in E_2 production, thus inhibiting the development of endometriotic lesions [7]. However, the hydroxyl groups on EGCG account for drug instability and result in low bioavailability in the body [21,22]. In contrast, ProEGCG can enhance this chemical stability by replacing the hydroxyl groups with acetyl groups [17]. This enables ProEGCG to demonstrate greater efficacy in inhibiting lesion development and suppressing angiogenic activities in endometriosis [14]. Our current study revealed that ProEGCG was more effective than EGCG as a preventive and treatment regimen for endometriosis, which can favor its clinical application. Recently, we used an *in silico* reverse screening approach and identified nicotinamide-nucleotide adenylyl transferases as binding targets of ProEGCG, which hypothetically played a role in increasing the antioxidant capacity of ProEGCG [18]. In addition, our current study identified the novel and distinct binding target profiles of EGCG and ProEGCG that contribute to the antiangiogenic mechanism for the prevention and treatment of endometriosis.

Compared to thermal proteome profiling, PISA exhibited more selectivity and specificity in drug target identification. The integral solubility approach of PISA enabled robust quantification of the total soluble proteome after a gradient of applied temperatures in a multiplex experiment, which would correspond to the integral of melting curves across these temperatures, simplifying and strengthening the quantitative data analysis. In contrast with the curve fitting approach by thermal proteome profiling, this would result in fewer statistical errors [19]. Our study adopted both 1D and 2D PISA, molecular docking studies and biolayer interferometry to confirm that MTDH bound to EGCG and PXK bound to ProEGCG. In addition, our study highlighted the intersecting protein targets to understand the mutual and differential therapeutic mechanisms and downstream signaling pathways of EGCG and ProEGCG in endometriosis. The establishment of knockdown models, followed by expression and functional studies, confirmed that the EGCG-MTDH-mediated Akt and ProEGCG-PXK-mediated EGF pathways are the targets and regulated pathways of EGCG and ProEGCG in endometriosis.

MTDH is known as Astrocyte Elevated Gene-1 and Lyric [23]. Although MTDH was found to increase metastasis risk in female reproductive cancers via the PI3K/Akt and nuclear factor kappa-light-chain-enhancer of activated B cells signaling pathways [24–27] and estrogen regulation [28], it has not been associated with endometriosis. MTDH promoted mitogen-activated protein kinase (MAPK) and VEGF-related pathways, stimulated epithelial–mesenchymal transition, cell invasiveness and angiogenesis via extracellular signal-regulated kinase 1/2 and Wnt signaling pathways, and regulated Ras, Akt and c-Myc [29] in cancers [30–34]. In endometrial cancer cells, MTDH activated the PI3K/Akt/mTOR pathway via PIP3 upregulation [35]. From our functional enrichment study, we demonstrated that MTDH regulated MYC and Akt-related pathways in endometriosis. These pathways have also been reported to induce VEGF and angiogenesis in endometriosis [36–38]. It has been shown that MTDH activates A1 and the PI3K/Akt pathway to further induce the activation of MTDH [39], VEGF and angiogenesis [32,40]. Likewise, a downregulated Akt1 level can inhibit VEGF expression and vessel formation [32,33,39]. Our *in vitro* and *in vivo* results concurrently showed that EGCG downregulated MTDH and Akt1 gene and protein expression levels (Table S6a). When MTDH was knocked down *in vitro* and *in vivo*, Akt1 expression was also downregulated (Table S6b). Similarly, EGCG regulated Akt1 via specific binding to MTDH (Fig. S14). Although ProEGCG downregulated MTDH, MYC and Akt1 to a greater extent than EGCG, these genes were not downregulated in the PXK knockdown model. Based on this observation, ProEGCG may regulate these genes via other pathways.

With PXK being highly conserved and ubiquitously expressed in humans, this is dependent on PI3K expression. When PI3K was inhibited, the endosomal localization of PXK was reported to be abolished [41]. As PXK is a multifunctional protein, it is responsible for endocytosis and cell migration via actin cytoskeletal reorganization [41]. It was also found to accelerate ligand-induced EGFR endocytosis [41]. However, PXK has not been studied for its role in endometriosis. This is the first study to demonstrate that ProEGCG bound to PXK and downregulated PXK and EGF-related pathways to inhibit the development and angiogenesis of endometriosis (Fig. S15). The decreased PXK level was shown to downregulate EGF expression. Although EGCG also regulated EGF expression, the effect was much less prominent. EGF binding to EGFR and enhanced

Fig. 5. Binding targets of *epigallocatechin* gallate (EGCG) and prodrug of *epigallocatechin* gallate (ProEGCG) *in vivo*. (A) Heatmaps of downstream genes expression profiles, metadherin (MTDH) and PXK, and downstream gene expression in endometriosis mice model after treatments of EGCG or ProEGCG respectively in microarray analysis. Fold change of targets and downstream in gene expression levels in endometriosis mice model after different treatments. Gene levels were normalized relative to control and *Gapdh* as housekeeping gene. Data show mean ± standard error of mean (SEM) ($n = 8$). (B) Representative images of immunohistochemistry (IHC) staining to determine protein expressions of targets and downstream proteins of EGCG in endometriotic lesions in different groups. IHC scoring system (H-Score) values in stromal cells. Data show mean ± SEM ($n = 4$). (C) Schematic diagram of knockdown mice model establishment. Representative images of the lesions after different treatments. Lesions size after treatments in endometriosis gene knockdown mice model. Data show mean ± SEM ($n = 12$). Fold change of targets and downstream in gene expression levels in endometriosis knock down mice model. Gene levels were normalized relative to control and Gapdh as housekeeping gene. Data show mean ± SEM ($n = 3$). (D) Representative images of Immunohistochemistry staining to determine protein expressions of targets and downstream proteins of EGCG in endometriotic lesions in different groups. H-Score values in stromal cells was shown. Data show mean ± SEM ($n = 4$). One-way analysis of variance (ANOVA) was used for the multiple group's comparisons, unpaired *t*-test for two groups comparison. $^{*}P < 0.05$, $^{**}P < 0.01$, $^{***}P < 0.001$, $^{****}P < 0.0001$, compared to control. VEGF: vascular endothelial growth factor; Akt: protein kinase B; MYC: Myc proto-oncogene protein; BLK: tyrosine-protein kinase; EGF: epidermal growth factor; siRNA: small interfering RNA.

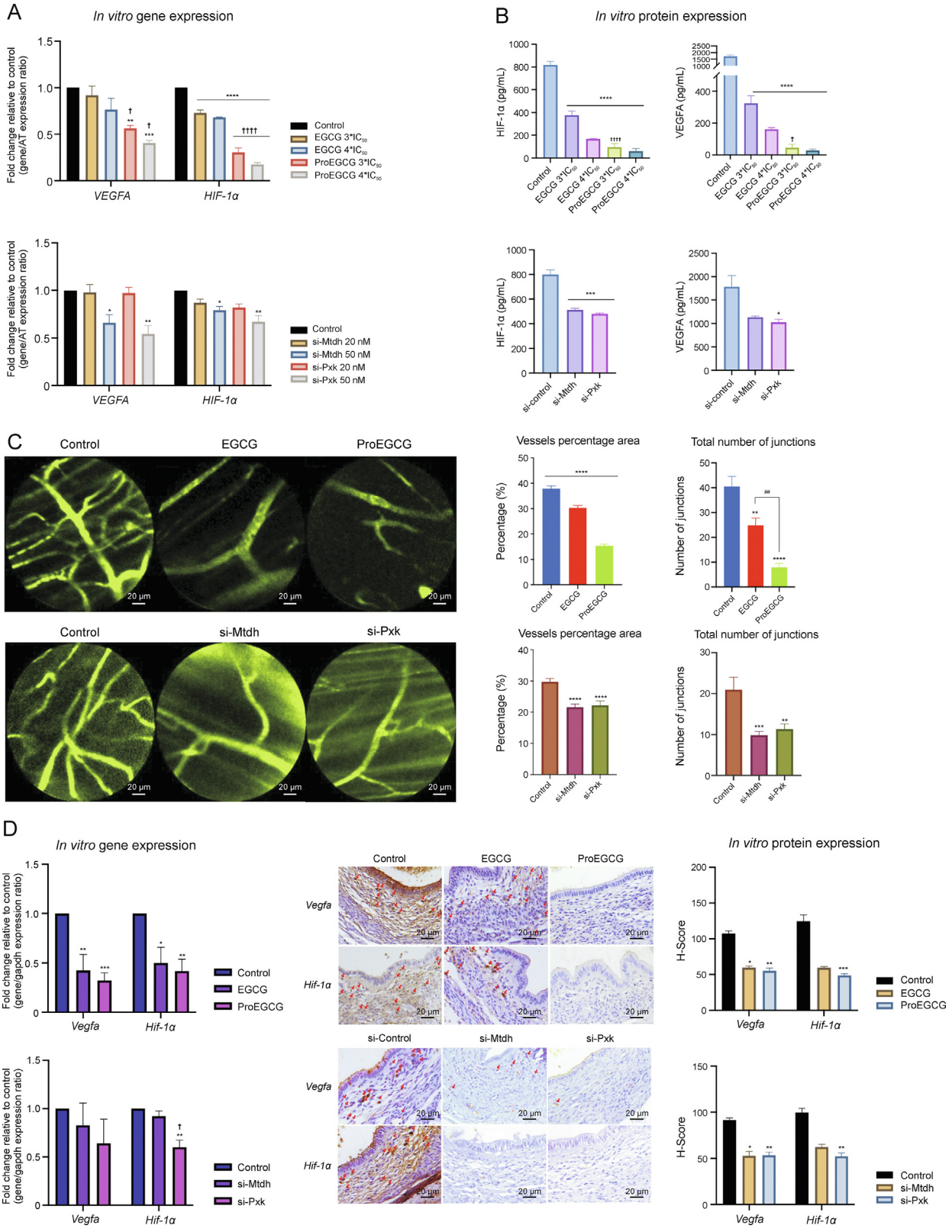

Fig. 6. Anti-angiogenic effects *in vitro* and *in vivo*. (A) Fold change of expression was normalized relative to housekeeping genes and control. Data show angiogenesis related genes *in vitro* after different treatments. Gene levels were normalized relative to housekeeping gene and control. Data show mean ± standard error of mean (SEM) (n = 3–4). (B) Enzyme-linked immunosorbent assay (ELISA) shows the hypoxia-inducible factor (HIF)-1α and vascular endothelial growth factor A (VEGFA) protein expression level changes after treatments. Data shows mean ± SEM (n = 3–4). (C) Representative images of micro vessel network *in vivo* after different treatments in endometriosis mice model. A total number of vessel junctions and length were measured by Angiotools. Data are represented by histograms and show mean ± SEM (n = 5). (D) (Left) Fold change of expression of angiogenesis related genes *in vivo* after different treatments in endometriosis model. Gene levels mean ± SEM (n = 3/8–9). (Middle) Representative images of the lesions after different treatments to show protein expressions of Vegfa and Hif-1α after different treatments. Red arrows denoted positive stained stromal cells. (Right) immunohistochemistry (IHC) scoring system (H-Score) values in stromal cells of lesions. Data show mean ± SEM (n = 6). One-way analysis of variance (ANOVA) with Tukey post-hoc test was used for all multiple group's comparison. $^{*}P < 0.05$, $^{**}P < 0.01$, $^{***}P < 0.001$, $^{****}P < 0.0001$, compared to control; $^{\#\#}P < 0.01$, compared to the same treatment at lower concentration; $^{\dagger}P < 0.05$, $^{\dagger\dagger\dagger\dagger}P < 0.0001$, compared to different treatments at the same concentration. PXK: PX domain containing serine/threonine kinase like; MTDH: metadherin.

receptor tyrosine kinase signaling pathways, including MAPK/ERK or PI3K/Akt/mTOR, play crucial roles in proliferation, migration, differentiation, and angiogenesis during the development of endometriosis [42,43]. Similarly, EGF levels in peritoneal fluid and endometriotic tissue of women with endometriosis have been reported to be increased and can cause dysregulated angiogenesis [44,45]. EGF also induces migration and invasion in endometriosis, as well as Akt phosphorylation, thus activating the PI3K/Akt signaling pathway [46].

Angiogenesis has been shown to regulate the development of endometriotic lesions [47,48] via HIF-1α activation to promote the VEGF signaling pathway [49]. EGF activation enhanced the activity of EGFR and the secretion of VEGF [50], as well as increased HIF-1α expression and its transcriptional activity via the PI3K/Akt pathway [51] or HIF-1α pathway [52]. The upregulation was found to be dose-dependent in activating angiogenesis [53]. ProEGCG treatment and the downregulated PXK level were shown to inhibit the growth of endometriotic lesions, angiogenic factors (VEGFA and HIF-1α) and microvascular network development more predominantly than EGCG or the downregulation of MTDH levels *in vitro* and *in vivo* (Table S6). Taken together, the exclusive and greater capacities of ProEGCG than EGCG could be explained as follows: 1) The binding of ProEGCG to PXK participated in the EGF/EGFR signaling pathways and inhibited EGF, HIF-1α, and VEGF expression levels via the HIF-1α pathway; 2) The binding of EGCG to MTDH participated in the PI3K/Akt pathway and inhibited MTDH and Akt1 expression. However, there was no significant HIF-1α expression level change when MTDH was inhibited. Similar to other literature findings [54,55], we reported that EGCG regulated VEGF and HIF-1α, but our study concluded that this was not by binding to MTDH in endometriosis.

This is the first study to demonstrate the superior efficacy of ProEGCG as a treatment and preventive regimen in endometriosis. The PISA-based proteomics approach demonstrated its ability to deconvolute the drug targets of EGCG and ProEGCG under different stability and solubility modifying factors (i.e., 6 treatment concentrations and 15 temperatures), thereby revealing the antiangiogenic-related mechanism of drug actions. This study had some limitations. First, we only selected 1 target each from EGCG and ProEGCG to carry out the in-depth functional studies. There might be other potential targets to be studied further. Second, PISA was carried out only in *in vitro* endometriotic cells. However, we had *in vivo* endometriosis models to validate the results and target expression, which helped to serve as an extrapolation of preclinical data into clinical reality. However, the subcutaneous endometriosis mouse model might not truly represent the lesion microenvironment. On the other hand, there were no currently available identified inhibitors that can bind to PXK or MTDH and could be used as positive drugs to compare the binding affinity with EGCG or ProEGCG. In addition, human samples are needed to further validate the mechanistic results and demonstrate the antiangiogenic effects of ProEGCG prior to clinical translation, as drug affinity might not necessarily be correlated with biological effect changes. Likewise, protein stability upon point mutations should also be measured to further support the findings. Third, we did not investigate the effect of drugs on downstream targets in knockout models. However, as EGCG and ProEGCG had other target candidates in endometriotic cells, as shown in PISA, they were shown to potentially regulate downstream targets via multiple pathways. Fourth, the binding of EGCG and ProEGCG to protein targets in different types of cells might trigger different chemical signals [56,57]. Finally, EGCG and ProEGCG might have different mechanistic actions when they interact with different cell types. Therefore, the crosstalk of the induced therapeutic effects of EGCG and ProEGCG in the microenvironment of endometriosis should be studied.

5. Conclusion

Our study was the first to identify distinct protein targets and mediated signaling pathways of EGCG and ProEGCG in treating endometriosis. The results suggested that EGCG bound to MTDH and inhibited Akt-mediated angiogenesis signal transduction, while ProEGCG bound to PXK and inhibited EGF-mediated angiogenesis effects. These findings help to reveal the novel binding targets and signal mechanism of EGCG and ProEGCG on the differentiated therapeutic efficacies to inhibit endometriosis progression and potentially justify the greater anti-endometriosis and anti-angiogenesis capacities of ProEGCG than EGCG.

CRediT author statement

Sze Wan Hung: Conceptualization, Methodology, Software, Validation, Formal analysis, Investigation, Data curation, Writing - Original draft preparation, Reviewing and Editing, Visualization; **Massimiliano Gaetani**: Conceptualization, Methodology, Software, Investigation, Resources, Data curation, Writing - Reviewing and Editing; **Yiran Li**: Methodology, Investigation, Validation; **Zhouyurong Tan**: Investigation, Validation; **Gene Chi Wai Man**: Methodology, Formal analysis, Investigation, Resources, Data curation, Writing - Reviewing and Editing; **Zheng Xu**: Investigation, Validation; **Ruizhe Zhang**: Investigation, Validation; **Yang Ding**: Investigation, Validation; **Tao Zhang**: Writing - Reviewing and Editing, Funding acquisition; **Yi Song**: Resources; **Yao Wang**: Writing - Reviewing and Editing; **Jacqueline Pui Wah Chung**: Resources, Writing - Reviewing and Editing; **Tak Hang Chan**: Resources, Writing - Reviewing and Editing; **Roman A. Zubarev**: Conceptualization, Resources, Writing - Reviewing and Editing, Supervision; **Chi Chiu Wang**: Conceptualization, Resources, Writing - Reviewing and Editing, Supervision, Funding acquisition

Declaration of competing interest

Chi Chiu Wang is an active member of the World Endometriosis Society and an advisor of Aptorum Group, the licensee of ProEGCG. Chi Chiu Wang and Chi Chiu Wang are the inventor of ProEGCG for endometriosis. The remaining authors declare that the research was conducted in the absence of any commercial or financial relationships that could be construed as a potential conflict of interest.

Acknowledgments

This work was supported by the GRF RGC & CRF, Hong Kong (Grant Nos.: 475012 and C5045-20 EF); HMRF, Hong Kong (Grant No.: 03141386); ITF, Hong Kong (Grant No.: ITS/209/12); UGC Direct Grant 2011,2012, 2021.032; HKOG Trust Fund 2011, 2014, 2019; and the National Natural Science Foundation of China (Grant Nos.: 81974225 and 82201823). The Chemical proteomics core facility at Biomedicum (MBB, Karolinska Institute), also the Unit of SciLifeLab and part of the Swedish National Infrastructure for Biological Mass Spectrometry (BioMS), provided full support in the experimental design and the performance of the proteomics analysis using the Proteome Integral Solubility Alteration (PISA) assay for target discovery, with relative data analysis.

Appendix A. Supplementary data

Supplementary data to this article can be found online at https://doi.org/10.1016/j.jpha.2023.09.005.

References

[1] K.T. Zondervan, C.M. Becker, S.A. Missmer, Endometriosis, N. Engl. J. Med. 382 (2020) 1244–1256.
[2] M.J. Fuldeore, A.M. Soliman, Prevalence and symptomatic burden of diagnosed endometriosis in the United States: National estimates from a cross-sectional survey of 59, 411 women, Gynecol. Obstet. Invest. 82 (2016) 453–461.
[3] J. Brown, C. Farquhar, Endometriosis: An overview of Cochrane Reviews, Cochrane Database Syst. Rev. (2014), CD009590.
[4] C.S. Deguara, B. Liu, C. Davis, Measured symptomatic and psychological outcomes in women undergoing laparoscopic surgery for endometriosis, Curr. Opin. Obstet. Gynecol. 25 (2013) 299–301.
[5] J.A. Sampson, Peritoneal endometriosis due to the menstrual dissemination of endometrial tissue into the peritoneal cavity, Am. J. Obstet. Gynecol. 14 (1927) 422–469.
[6] L.F. Jerman, A.J. Hey-Cunningham, The role of the lymphatic system in endometriosis: A comprehensive review of the literature, Biol. Reprod. 92 (2015) 64 1–10.
[7] S.W. Hung, R. Zhang, Z. Tan, et al., Pharmaceuticals targeting signaling pathways of endometriosis as potential new medical treatment: A review, Med. Res. Rev. 41 (2021) 2489–2564.
[8] G. Bozdag, Recurrence of endometriosis: risk factors, mechanisms and biomarkers, Women's Heath 11 (2015) 693–699.
[9] G. Grandi, F. Barra, S. Ferrero, et al., Hormonal contraception in women with endometriosis: a systematic review, Eur. J. Contracept. Reprod. Health Care 24 (2019) 61–70.
[10] D. Scholes, A.Z. LaCroix, L.E. Ichikawa, et al., Change in bone mineral density among adolescent women using and discontinuing depot medroxyprogesterone acetate contraception, Arch. Pediatr. Adolesc. Med. 159 (2005) 139–144.
[11] H.S. Taylor, L.C. Giudice, B.A. Lessey, et al., Treatment of endometriosis-associated pain with elagolix, an oral GnRH antagonist, N. Engl. J. Med. 377 (2017) 28–40.
[12] W. Zheng, L. Cao, Z. Xu, et al., Anti-angiogenic alternative and complementary medicines for the treatment of endometriosis: A review of potential molecular mechanisms, Evid. Based Complementary Altern. Med. 2018 (2018) 1–28.
[13] Y. Que, Y. Liang, J. Zhao, et al., Treatment-related adverse effects with pazopanib, sorafenib and sunitinib in patients with advanced soft tissue sarcoma: A pooled analysis, Cancer Manag. Res. 10 (2018) 2141–2150.
[14] C.C. Wang, H. Xu, G.C.W. Man, et al., Prodrug of green tea epigallocatechin-3-gallate (Pro-EGCG) as a potent anti-angiogenesis agent for endometriosis in mice, Angiogenesis 16 (2013) 59–69.
[15] H. Xu, C.M. Becker, W.T. Lui, et al., Green tea epigallocatechin-3-gallate inhibits angiogenesis and suppresses vascular endothelial growth factor C/vascular endothelial growth factor receptor 2 expression and signaling in experimental endometriosis *in vivo*, Fertil. Steril. 96 (2011) 1021–1028.e1.
[16] H. Xu, W.T. Lui, C.Y. Chu, et al., Anti-angiogenic effects of green tea catechin on an experimental endometriosis mouse model, Hum. Reprod. 24 (2009) 608–618.
[17] W.H. Lam, A. Kazi, D.J. Kuhn, et al., A potential prodrug for a green tea polyphenol proteasome inhibitor: evaluation of the peracetate ester of (−)-epigallocatechin gallate [(−)-EGCG, Bioorg. Med. Chem. 12 (2004) 5587–5593.
[18] S.W. Hung, B. Liang, Y. Gao, et al., An In-silico, *In-vitro* and *in-vivo* combined approach to identify NMNATs as potential protein targets of ProEGCG for treatment of endometriosis, Front. Pharmacol. 12 (2021), 714790.
[19] M. Gaetani, P. Sabatier, A.A. Saei, et al., Proteome integral solubility alteration: A high-throughput proteomics assay for target deconvolution, J. Proteome Res. 18 (2019) 4027–4037.
[20] T. Tang, Y. Deng, J. Chen, et al., Local administration of siRNA through microneedle: optimization, bio-distribution, tumor suppression and toxicity, Sci. Rep. 6 (2016), 30430.
[21] G. Du, Z. Zhang, X. Wen, et al., Epigallocatechin gallate (EGCG) is the most effective cancer chemopreventive polyphenol in green tea, Nutrients 4 (2012) 1679–1691.
[22] C. Chu, J. Deng, Y. Man, et al., Green tea extracts epigallocatechin-3-gallate for different treatments, BioMed Res. Int. 2017 (2017), 5615647.
[23] H.J. Thirkettle, J. Girling, A.Y. Warren, et al., LYRIC/AEG-1 is targeted to different subcellular compartments by ubiquitinylation and intrinsic nuclear localization signals, Clin. Cancer Res. 15 (2009) 3003–3013.
[24] Y. Hou, L. Yu, Y. Mi, et al., Association of MTDH immunohistochemical expression with metastasis and prognosis in female reproduction malignancies: A systematic review and meta-analysis, Sci. Rep. 6 (2016), 38365.
[25] J. Mazieres, T. Antonia, G. Daste, et al., Loss of RhoB expression in human lung cancer progression, Clin. Cancer Res. 10 (2004) 2742–2750.
[26] G. Hu, Y. Wei, Y. Kang, The multifaceted role of MTDH/AEG-1 in cancer progression, Clin. Cancer Res. 15 (2009) 5615–5620.
[27] X. Shi, X. Wang, The role of MTDH/AEG-1 in the progression of cancer, Int. J. Clin. Exp. Med. 8 (2015) 4795–4807.
[28] Y. Li, J.G. Bosquet, S. Yang, et al., Role of metadherin in estrogen-regulated gene expression, Int. J. Mol. Med. 40 (2017) 303–310.
[29] D. Manna, D. Sarkar, Multifunctional role of astrocyte elevated gene-1 (AEG-1) in cancer: focus on drug resistance, Cancers 13 (2021), 1792.
[30] S.G. Lee, Z.Z. Su, L. Emdad, et al., Astrocyte elevated gene-1 activates cell survival pathways through PI3K-Akt signaling, Oncogene 27 (2008) 1114–1121.
[31] L. Emdad, D. Sarkar, Z. Su, et al., Activation of the nuclear factor κB pathway by astrocyte elevated gene-1: Implications for tumor progression and metastasis, Cancer Res. 66 (2006) 1509–1516.
[32] L. Emdad, S.G. Lee, Z. Su, et al., Astrocyte elevated gene-1 (AEG-1) functions as an oncogene and regulates angiogenesis, Proc. Natl. Acad. Sci. U.S.A. 106 (2009) 21300–21305.
[33] G. Zhu, C. Yu, L. She, et al., Metadherin regulation of vascular endothelial growth factor expression is dependent upon the PI3K/akt pathway in squamous cell carcinoma of the head and neck, Medicine 94 (2015), e502.
[34] J. Yang, Z. Wang, Z. Tang, et al., Metadherin regulates epithelial-mesenchymal transition in carcinoma, OncoTargets Ther. (2016), 2429.
[35] X. Meng, P. Brachova, S. Yang, et al., Knockdown of MTDH sensitizes endometrial cancer cells to cell death induction by death receptor ligand TRAIL and HDAC inhibitor LBH589 co-treatment, PLoS One 6 (2011), e20920.
[36] J. Guo, J. Gao, X. Yu, et al., Expression of DJ-1 and mTOR in eutopic and ectopic endometria of patients with endometriosis and adenomyosis, Gynecol. Obstet. Invest. 79 (2015) 195–200.
[37] K.R. Rogers-Broadway, J. Kumar, C. Sisu, et al., Differential expression of mTOR components in endometriosis and ovarian cancer: Effects of rapalogues and dual kinase inhibitors on mTORC1 and mTORC2 stoichiometry, Int. J. Mol. Med. 43 (2019) 47–56.
[38] Y. Mizukami, K. Fujiki, E.M. Duerr, et al., Hypoxic regulation of vascular endothelial growth factor through the induction of phosphatidylinositol 3-kinase/rho/ROCK and c-myc, J. Biol. Chem. 281 (2006) 13957–13963.
[39] L. Emdad, S.K. Das, S. Dasgupta, et al., AEG-1/MTDH/LYRIC: Signaling pathways, downstream genes, interacting proteins, and regulation of tumor angiogenesis, Adv. Cancer Res. 120 (2013) 75–111.
[40] C. Blancher, J.W. Moore, N. Robertson, et al., Effects of ras and von Hippel-Lindau (VHL) gene mutations on hypoxia-inducible factor (HIF)-1alpha, HIF-2alpha, and vascular endothelial growth factor expression and their regulation by the phosphatidylinositol 3'-kinase/Akt signaling pathway, Cancer Res. 61 (2001) 7349–7355.
[41] H. Takeuchi, T. Takeuchi, J. Gao, et al., Characterization of PXK as a protein involved in epidermal growth factor receptor trafficking, Mol. Cell Biol. 30 (2010) 1689–1702.
[42] F. Zeng, R.C. Harris, Epidermal growth factor, from gene organization to bedside, Semin. Cell Dev. Biol. 28 (2014) 2–11.
[43] Y. Wang, M. Wu, Y. Lin, et al., Association of epidermal growth factor receptor (EGFR) gene polymorphisms with endometriosis, Medicine 98 (2019), e15137.
[44] R.E.B. Haining, I.T. Cameron, C. van Papendorp, et al., Epidermal growth factor in human endometrium: Proliferative effects in culture and immunocytochemical localization in normal and endometriotic tissues, Hum. Reprod. 6 (1991) 1200–1205.
[45] H. Rakhila, M. Al-Akoum, M.E. Bergeron, et al., Promotion of angiogenesis and proliferation cytokines patterns in peritoneal fluid from women with endometriosis, J. Reprod. Immunol. 116 (2016) 1–6.
[46] H. Zhan, B. Peng, J. Ma, et al., Epidermal growth factor promotes stromal cells migration and invasion via up-regulation of hyaluronate synthase 2 and hyaluronan in endometriosis, Fertil, Steril 114 (2020) 888–898.
[47] R.N. Taylor, J. Yu, P.B. Torres, et al., Mechanistic and therapeutic implications of angiogenesis in endometriosis, Reprod. Sci. 16 (2009) 140–146.
[48] A.W. Nap, A.W. Griffioen, G.A.J. Dunselman, et al., Antiangiogenesis therapy for endometriosis, J. Clin. Endocrinol. Metab. 89 (2004) 1089–1095.
[49] C.M. Becker, N. Rohwer, T. Funakoshi, et al., 2-methoxyestradiol inhibits hypoxia-inducible factor-1α and suppresses growth of lesions in a mouse model of endometriosis, Am. J. Pathol. 172 (2008) 534–544.
[50] C.K. Goldman, J. Kim, W.L. Wong, et al., Epidermal growth factor stimulates vascular endothelial growth factor production by human malignant glioma cells: a model of glioblastoma multiforme pathophysiology, Mol. Biol. Cell 4 (1993) 121–133.
[51] H. Zhong, K. Chiles, D. Feldser, et al., Modulation of hypoxia-inducible factor 1alpha expression by the epidermal growth factor/phosphatidylinositol 3-kinase/PTEN/AKT/FRAP pathway in human prostate cancer cells: implications for tumor angiogenesis and therapeutics, Cancer Res. 60 (2000) 1541–1545.
[52] N. Pore, Z. Jiang, A. Gupta, et al., EGFR tyrosine kinase inhibitors decrease VEGF expression by both hypoxia-inducible factor (HIF)-1–independent and HIF-1–dependent mechanisms, Cancer Res. 66 (2006) 3197–3204.
[53] D. Zepeda-Orozco, H.M. Wen, B.A. Hamilton, et al., EGF regulation of proximal tubule cell proliferation and VEGF-A secretion, Phys. Rep. 5 (2017), e13453.
[54] Q. Zhang, X. Tang, Q. Lu, et al., Green tea extract and (−)-epigallocatechin-3-gallate inhibit hypoxia- and serum-induced HIF-1α protein accumulation and VEGF expression in human cervical carcinoma and hepatoma cells, Mol. Cancer Therapeut. 5 (2006) 1227–1238.
[55] H. Luo, M. Xu, W. Zhong, et al., EGCG decreases the expression of HIF-1α and VEGF and cell growth in MCF-7 breast cancer cells, J. Buon 19 (2014) 435–439.
[56] M. Mittelbrunn, F. Sánchez-Madrid, Intercellular communication: diverse structures for exchange of genetic information, Nat. Rev. Mol. Cell Biol. 13 (2012) 328–335.
[57] B.L.D.M. Brücher, I.S. Jamall, Cell-cell communication in the tumor microenvironment, carcinogenesis, and anticancer treatment, Cell. Physiol. Biochem. 34 (2014) 213–243.